Article

# Alloyed PdCu Nanoparticles within Siliceous Zeolite Crystals for Catalytic Semihydrogenation

Qingsong Luo,[†] Hai Wang,[†] Liang Wang,* and Feng-Shou Xiao*

Cite This: *ACS Mater. Au* 2022, 2, 313−320

Read Online

ACCESS | ⏸ Metrics & More | 📖 Article Recommendations | SI Supporting Information

**ABSTRACT:** Selective hydrogenation of acetylene to ethylene is an industrially important process to purify the raw ethylene stream for producing high-grade polyethylene. The supported Pd catalyst exhibits superior activity for acetylene hydrogenation but suffers from poor ethylene selectivity because of the easy overhydrogenation to produce ethane. Here, we report that the PdCu alloy nanoparticles within siliceous zeolite crystals effectively tuned Pd-catalyzed overhydrogenation into semihydrogenation. This catalyst displayed an ethylene selectivity of 92.9% with a full conversion of acetylene. Mechanism studies reveal that the zeolite fixation stabilized the alloyed structure, where the electron-enriched Pd surface benefits the rapid ethylene desorption to hinder the deep hydrogenation. This work provides an efficient strategy for a rational design of bimetallic metal catalysts for selective hydrogenations.

**KEYWORDS:** metal alloy, zeolite, fixed structure, acetylene semihydrogenation
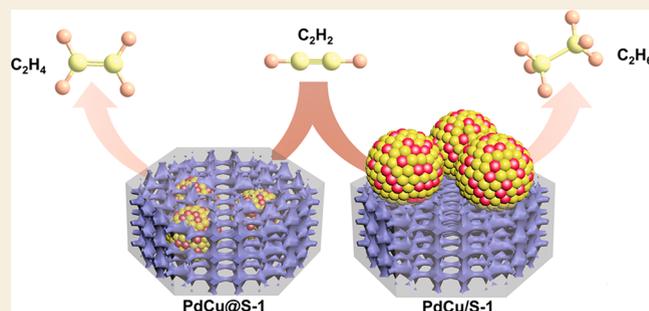
## ■ INTRODUCTION

Ethylene ($C_2H_4$) has been regarded as one of the most important platform molecules for producing polyethylene and other valuable chemicals.[1] The current $C_2H_4$ production relies on steam reforming of naphtha, which usually coproduces a slight amount of acetylene ($C_2H_2$, 0.6−2%) in $C_2H_4$,[2−4] which would poison the Ziegler−Natta catalyst in the following $C_2H_4$ polymerization process.[5,6] Selective removal of $C_2H_2$ is always required to obtain polyethylene with a polymerization grade purity. With regard to this issue, a promising strategy is to selectively hydrogenate the $C_2H_2$ into $C_2H_4$ to eliminate the poison effect on the Ziegler−Natta catalyst.[7−9] Pd-based catalysts are usually employed because of the high reactivity for hydrogenation.[10,11] Unfortunately, the facile formation of $PdH_x$ hydride and strong adsorption of $C_2H_4$ over Pd catalysts can inevitably lead to deep hydrogenation of $C_2H_4$, thus reducing and even losing the catalytic activity.[12,13] To solve this problem, other metal components such as Ag,[14−16] Cu,[17] Zn,[18] Ga,[19,20] In,[21,22] and Au[23] are subsequently used to modify the electronic and geometric structures of Pd to alter its catalytic performances. Although significantly improved catalytic selectivity has been successfully achieved, the synthesis of these alloys still requires a finely controlled procedure to avoid the easy phase separation during the metal deposition processes.[24] In addition, the alloy metal nanoparticles (NPs) also suffer from metal sintering and phase separation during the reaction or catalyst regeneration under harsh conditions (e.g., high temperature and hydrogen-rich environment).[25] As a result, the alloyed structure is inevitably

destroyed to lose the desired catalytic performance. In addition to the metal NP structures, the local environment of metal species is also important, which is expected to control the competitive sorption of $C_2H_4$ and $C_2H_2$ to optimize the reaction selectivity.[26] However, this feature is sometimes ignored in the catalyst design.

Herein, we report an efficient strategy to optimize the selectivity of Pd-based catalyst in semihydrogenation, which is realized by fixing the PdCu NPs within the zeolite crystals. Because the zeolite has a rigid framework and thermally stable structure, the sintering and phase separation of these alloyed NPs are efficiently avoided under various redox conditions. The zeolite micropores allow access of reactant molecules to the metal surface, facilitating catalytic hydrogenation reactions. More importantly, the zeolite fixed structure benefits the rapid desorption of $C_2H_4$ product to minimize deep hydrogenation. The combination of metal active sites with zeolite structure provides an effective way to control the product selectivity. Following these features, the $C_2H_4$ selectivity reaches 92.9% with a full conversion of $C_2H_2$ in the siliceous MFI zeolite fixed PdCu catalyst (PdCu@S-1), and such performances were well-maintained in a continuous reaction for a long period of time.
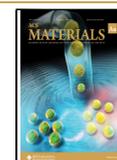
## ■ MATERIALS AND METHODS

### Chemical Reagents

All of the chemicals were used as received without further purification. Tetrapropylammonium hydroxide (TPAOH, 40 wt %) was supplied by Shanghai Cairui Chemical Technology Co. Ltd. Tetraethylorthosilicate (TEOS, >99%) was purchased from Aladdin Chemical Reagent Company. $Na_2PdCl_4$ (99%) was purchased from Beijing HWRK Chem Co. Ltd. $Cu(NO_3)_2 \cdot 3H_2O$ (AR), ethylenediamine (AR), and hydrofluoric acid (AR, 40 wt %) were purchased from Sinopharm Chemical Reagent.

### Synthesis

**Synthesis of S-1.** First, 14.88 g of TPAOH (40 wt %) was added into 90.24 g of deionized water and stirred for 10 min. Then 26.16 g of TEOS was slowly added into the mixture and stirred at room temperature for another 6 h. The solution was transferred into an autoclave and heated at 180 °C for 4 days. After removal of the organic template by calcination at 550 °C for 4 h in air, the S-1 zeolite was obtained.

**Synthesis of PdCu@S-1.** First, 14.88 g of TPAOH (40 wt %) was added into 90.24 g of deionized water and stirred for 10 min in flask A. Then 26.16 g of TEOS was slowly added into the solution and stirred at room temperature for 6 h to obtain a clear and transparent solution. Next, 0.75 mL of $Na_2PdCl_4$ (20 mg/mL) and 0.285 g of $Cu(NO_3)_2 \cdot 3H_2O$ were dissolved in 5 mL of deionized water in flask B and stirred for 30 min. Then 0.606 g of ethylenediamine was then added into the above solution and stirred for another 30 min. After that, the liquor in flask B was added into flask A under stirring, followed by stirring at room temperature for 10 min. Finally, the solution was transferred into an autoclave and heated at 180 °C for 4 days. After removal of the organic template by calcination at 550 °C for 4 h in air, the PdCu@S-1 sample was obtained.

**Synthesis of Pd@S-1.** First, 14.88 g of TPAOH (40 wt %) was added into 90.24 g of deionized water and stirred for 10 min in flask A. Then 26.16 g of TEOS was slowly dropped into the above solution and stirred at room temperature for 6 h to obtain a clear and transparent solution. Next, 0.75 mL of $Na_2PdCl_4$ (20 mg/mL) was dissolved in 5 mL of deionized water in flask B and stirred for 30 min. Then 0.606 g of ethylenediamine was added into the above solution and stirred for another 30 min. After that, the liquor in flask B was added into flask A under stirring, followed by stirring at room temperature for another 10 min. Finally, the solution was transferred into an autoclave and heated at 180 °C for 4 days. After removal of the organic template by calcination at 550 °C for 4 h in air, Pd@S-1 was obtained.

**Synthesis of Cu@S-1.** First, 14.88 g of TPAOH (40 wt %) was added into 90.24 g of deionized water and stirred for 10 min in flask A. Then 26.16 g of TEOS was slowly dropped into the above solution and stirred at room temperature for 6 h to obtain a clear and transparent solution. Next, 0.285 g of $Cu(NO_3)_2 \cdot 3H_2O$ was dissolved in 5 mL of deionized water in flask B and stirred for 30 min. Then 0.606 g of ethylenediamine was added into the above solution and stirred for another 30 min. The liquor in flask B was added into flask A under stirring, followed by stirring at room temperature for another 10 min. Finally, the solution was transferred into an autoclave and heated at 180 °C for 4 days. After removal of the organic template by calcination at 550 °C for 4 h in air, Cu@S-1 was obtained.

**Synthesis of PdCu/S-1.** First, 0.10 mL of $Na_2PdCl_4$ (20 mg/mL) and 0.058 g of $Cu(NO_3)_2 \cdot 3H_2O$ were dissolved in 50 mL of deionized water and stirred for 10 min at room temperature. Then 1.0 g of S-1 was added into the above solution and stirred for 12 h. Finally, the water in the mixture was removed by rotary evaporation to obtain solid powder. After being dried at 60 °C for 12 h and calcination at 400 °C for 2 h, PdCu/S-1 was obtained.

**Synthesis of Cu/S-1.** First, 0.032 g of $Cu(NO_3)_2 \cdot 3H_2O$ was dissolved in 50 mL of deionized water and stirred for 10 min at room temperature. Then 1.0 g of S-1 was added into the above solution and stirred for 12 h. Finally, the water in the mixture was removed by rotary evaporation to obtain solid powder. After being dried at 60 °C for 12 h and calcination at 400 °C for 2 h, the Cu/S-1 was obtained.

**Synthesis of PdCu@S-1-HF.** First, 1.0 g of PdCu@S-1 was stirred in 5 mL of hydrofluoric acid (HF) solution (1 wt %) at room temperature for 10 min and then filtered, washed, and dried at 100 °C for 12 h to obtain the final HF-treated PdCu@S-1 catalyst, which was denoted as PdCu@S-1-HF.

### Characterization

The details for X-ray diffraction (XRD), inductively coupled plasma (ICP), X-ray photoelectron spectroscopy (XPS), thermogravimetric (TG), and transmission electron microscopy (TEM) characterizations are given in the Supporting Information.

In situ Fourier transform infrared (FTIR) spectra of CO adsorptions were recorded using a Vertex 70 equipped with an in situ heating chamber. Before CO adsorption, the catalysts were first reduced at 400 °C for 2 h in 10 vol % $H_2/Ar$ (20 mL/min) and then cooled to room temperature. The background spectrum was collected in a continuous Ar flow. A mixed gas of 10 vol % CO in He (20 mL/min) was subsequently introduced into the sample chamber, and the spectra were collected with time until there was no change in the signals. After that, helium was introduced into the in situ chamber for different periods to detect the change of the CO signals.

In situ $C_2H_2$ adsorption FTIR characterizations were carried out on a Vertex 70 equipped with an in situ heating chamber. The catalysts were first reduced at 400 °C for 2 h in 10 vol % $H_2/Ar$ (20 mL/min) and then cooled to room temperature. The background spectrum was collected in the continuous Ar flow. Then a 5 vol % $C_2H_2$ in Ar was introduced into the catalysts, and the IR spectra were recorded. Subsequently, a flow of 0.2 vol % $C_2H_2/9.5$ vol %$H_2/Ar$ was introduced, and the spectrum was recorded with time until there was no visible change in the intensities of the absorption band.

Mass spectra of the effluent gases introduced into a flow system or produced by reaction with the sample were measured on a mass spectrometer (SRD200M, Tilon GRP Technology Limited) instrument connected to a reaction tube that was heated by an oven. Typically, the catalysts were first reduced at 400 °C for 2 h in 10 vol % $H_2/Ar$ (20 mL/min) and then cooled to room temperature. Subsequently, 5 vol % $C_2H_2$ or 20 vol % $C_2H_4$ was introduced for 1 h (40 mL/min), and He was introduced to purge excess gas until there was no change in the signals. The oven was heated to 500 °C at 5 °C/min, and MS signals were collected with increasing the temperatures.

### Catalysis

The semihydrogenation of $C_2H_2$ was performed in a continuous-flow fixed-bed reactor with a quartz tube (7.4 mm i.d., 270 mm long) at a constant total pressure (0.1 MPa). Typically, 30 mg of the catalyst (40−60 mesh) diluted with quartz sand (40−60 mesh) was localized in the middle of the reactor. The catalyst was pretreated in 20 vol % $H_2/Ar$ at 400 °C for 2 h and cooled to the desired reaction temperature. Subsequently, a reactant gas mixture containing 1 vol % $C_2H_2/10$ vol % $H_2/Ar$ or 1 vol % $C_2H_2/10$ vol % $H_2/30$ vol % $C_2H_4/Ar$ was fed into the reactor. The total flow rate was controlled at 20 mL/min, corresponding to a gas hourly space velocity (GHSV) of 40000 mL $g_{cat}^{-1}$ $h^{-1}$. The reaction outlet was analyzed online by a gas chromatograph equipped with a PLOT $Al_2O_3$ capillary column and a flame ionization detector.

$C_2H_2$ conversion was calculated as follows:[27]

$$\text{conversion} = \frac{C_2H_2(\text{feed}) - C_2H_2}{C_2H_2(\text{feed})} \times 100\%$$

Selectivity to $C_2H_4$ was calculated as follows:[27]

For $C_2H_4$ free atmosphere:

$$\text{selectivity} = \frac{C_2H_4}{C_2H_4 + C_2H_6 + 2C_4\text{olefin}} \times 100\%$$

For $C_2H_4$-rich atmosphere:[27]

$$\text{selectivity} = \frac{C_2H_2(\text{feed}) - C_2H_2}{C_2H_2(\text{feed}) - C_2H_2 + C_2H_6 + 2C_4\text{olefin}} \times 100\%$$

## ■ RESULTS AND DISCUSSION

### Synthesis and Characterization

Because the aluminosilicate zeolites containing acidic sites lead to the undesired side reaction of ethylene oligomerization,[14] the siliceous zeolite was chosen to fix the PdCu nanoparticles in this work. A series of silicate-1 (S-1) zeolite fixed metal catalysts (M@S-1) were prepared through a hydrothermal route (M = Pd, Cu, or PdCu; see the Materials and Methods section for details). For achieving the zeolite fixed structure, strong interactions between the metal species and zeolite precursors are crucial.[28−30] We employed ethylenediamine to stabilize the palladium and copper species in the zeolite crystallization gel in strong alkaline media, which could avoid metal aggregation under the high crystallization temperature.[28] Meanwhile, the ethylenediamine could also strongly interact with the silica species to ensure the formation of a zeolite fixed structure.[30] After calcination to remove the organic template and ethylenediamine species, the M@S-1 samples were obtained. The synthesis procedures are summarized in Scheme 1.

**Scheme 1. Synthetic Procedure of PdCu@S-1**
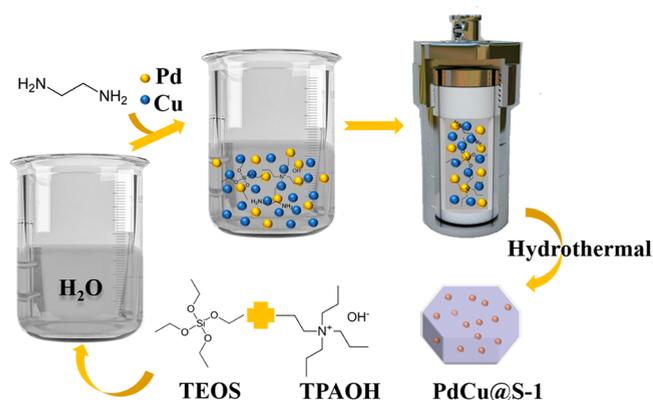


Supporting Information Figure S1 shows XRD patterns of the S-1 zeolite and various S-1-supported metal catalysts, giving peaks of typical MFI zeolite structure. The characteristic peaks of metallic Pd and/or Cu were not observed, which is due to the low loadings and/or high dispersions of these species. N$_2$ sorption isotherms of PdCu@S-1 exhibited a type-I curve and high specific surface areas (Supporting Information Figure S2 and Table 1), supporting the high crystallinity. The scanning electron microscopy (SEM) images of PdCu@S-1,

Pd@S-1, Cu@S-1, and PdCu/S-1 (Figure 1a and Supporting Information Figure S3) gave the zeolite crystals with a uniform morphology and size distribution (200−500 nm). These data confirm the successful synthesis of the MFI zeolite.

TEM characterizations provide a direct observation of metal NPs within zeolite crystals. TEM images of PdCu@S-1, Pd@S-1, and Cu@S-1 clearly show the metal NPs within the S-1 zeolite region (Figure 1b and Supporting Information Figures S4 and S5), and the particles on the external zeolite region were undetectable. For comparison, we also synthesized the metal NPs on the S-1 zeolite crystals via a conventional deposition method, giving PdCu/S-1 with metal NPs mostly localized on the edges of the S-1 support (Supporting Information Figure S6), indicating that the NPs are on the external surface of the zeolite crystal. The alloyed structure of PdCu in PdCu@S-1 was evidenced by a linear scan (Figure 1c) and energy-dispersive spectroscopy elemental maps (Figure 1d−i), showing the highly consistent Pd and Cu elemental distribution. The average size of PdCu NPs in PdCu@S-1 was 3.9 nm (Figure 1b and Table 1), which was obviously larger than the diameter of zeolite micropores, confirming the fixed structure. In this case, the metal NPs have to break the zeolite framework and cross several micropores and were immobilized by the rigid zeolite crystals.[29] The Pd@S-1 without Cu species showed the average Pd NP size at 3.2 nm (Supporting Information Figure S4 and Table 1). These data verify the successful formation of a PdCu alloy structure within the zeolite crystals. As PdCu@S-1 was obtained by calcination at a high temperature of 550 °C in air, the small PdCu NP sizes demonstrate its good sinter resistance. In contrast, the metal NPs on PdCu/S-1 sintered considerably after the calcination treatment (Supporting Information Figure S6), which is related to the lack of zeolite sheath for stabilizing the metal NPs.

### Catalysis

The catalysts were evaluated in C$_2$H$_2$ semihydrogenation under given reaction conditions (1 vol % C$_2$H$_2$/10 vol % H$_2$/89 vol % Ar, GHSV = 40000 mL g$^{-1}$ h$^{-1}$) in Figure 2. The Pd@S-1 exhibited C$_2$H$_2$ conversion of 98.0% with C$_2$H$_4$ selectivity of 46.9% at 75 °C. Increasing the reaction temperature caused a dramatic decrease of the C$_2$H$_4$ selectivity with C$_2$H$_6$ as a dominant product because of the deep hydrogenation of C$_2$H$_4$ (Supporting Information Figure S7 and Table S1). Interestingly, addition of Cu to the Pd catalysts significantly increased the C$_2$H$_4$ selectivity. For example, 92.9% selectivity of C$_2$H$_4$ was obtained under 94.8% conversion of C$_2$H$_2$ at 175 °C over the PdCu@S-1 catalyst (Figure 2 and Supporting Information Figure S8 and Table S1). In this case, the catalytic activity was decreased compared with the Pd@S-1 catalyst, which is in agreement with the general phenomenon

**Table 1. Structural Parameters of Various Catalysts and Their Performances in Acetylene Semihydrogenation**

| catalyst | Pd loading (wt %)[a] | Cu loading (wt %)[a] | metal size (nm) | $S_{BET}$ (m$^2$/g) | pore volume (cm$^3$/g) | temp (°C)[b] | ethylene sel. (%)[c] | average rate (mol$_{acetylene}$ mol$_{Pd}$$^{-1}$ h$^{-1}$)[d] |
|---|---|---|---|---|---|---|---|---|
| PdCu@S-1 | 0.11 | 0.77 | 3.9 | 409.5 | 0.25 | 175 | 92.9 | 1273.0 |
| Pd@S-1 | 0.10 | | 3.2 | 393.1 | 0.26 | 75 | 52.7 | 1854.4 |
| Cu@S-1 | | 0.84 | | 375.0 | 0.20 | | | |
| PdCu/S-1 | 0.10 | 1.51 | | 366.2 | 0.24 | 125 | 76.3 | 1755.6 |

[a]Determined by ICP analysis. [b]The reaction temperature corresponding to the complete conversion of acetylene. Reaction conditions: 1 vol % C$_2$H$_2$, 10 vol % H$_2$, Ar, GHSV at 40000 mL g$^{-1}$ h$^{-1}$. [c]The ethylene selectivity corresponding to the nearly complete conversion of acetylene. Reaction conditions: 1 vol % C$_2$H$_2$, 10 vol % H$_2$, Ar, GHSV at 40000 mL g$^{-1}$ h$^{-1}$. [d]Calculated based on the total amount of Pd.
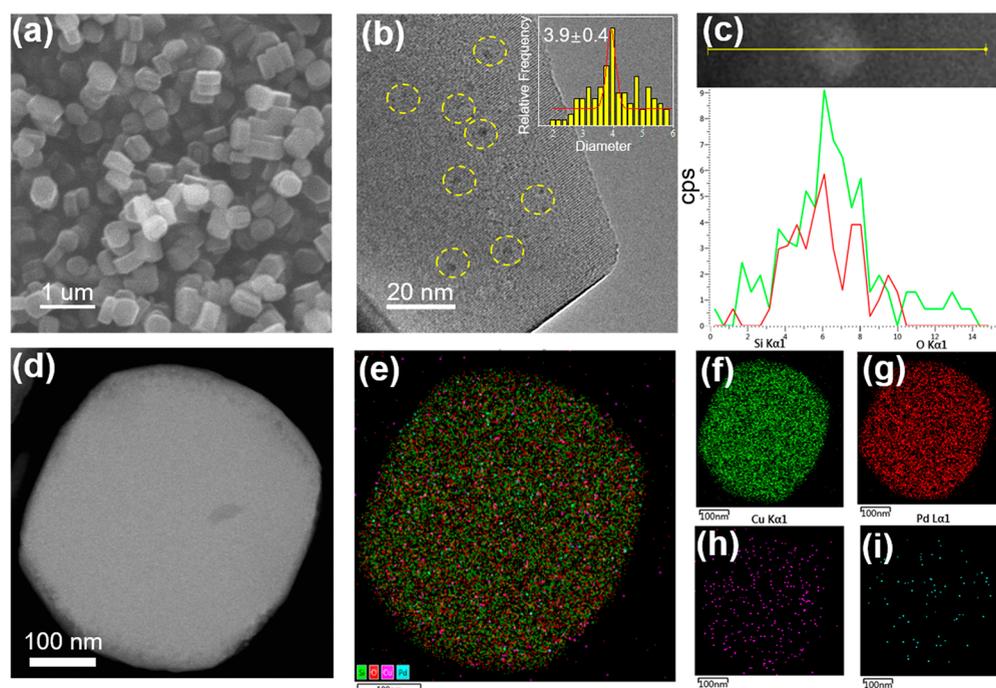
**Figure 1.** (a) SEM and (b) TEM images of PdCu@S-1. Inset in (b): metal NP size distribution. (c) Linear scan of the alloyed NP. (d−i) Scanning transmission electron microscopy image and the corresponding element maps showing distributions of Si (f), O (g), Cu (h), and Pd (i) of PdCu@S-1.
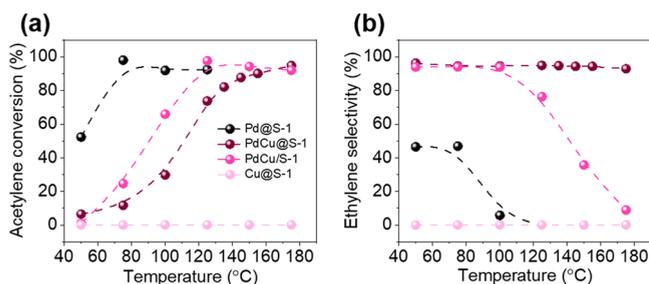


**Figure 2.** (a) $C_2H_2$ conversion and (b) $C_2H_4$ selectivity as a function of reaction temperature in the $C_2H_2$ semihydrogenation over various catalysts. Reaction conditions: 1 vol % $C_2H_2$, 10 vol % $H_2$, Ar, GHSV at 40000 mL $g^{-1}$ $h^{-1}$.

on modified Pd catalysts for semihydrogenation.[14,17−19] Notably, the Cu@S-1 catalyst was almost inactive for the $C_2H_2$ hydrogenation in a wide temperature range (50−180 °C, Figure 2) due to the very low Cu loading in the Cu@S-1 (0.8 wt % Cu). The Cu/S-1 catalyst with 0.8 wt % Cu loading has very low activity (Supporting Information Figure S9), in good agreement with the those on the supported Cu catalyst tested previously.[31] By contrast, general active catalysts have high Cu loadings even higher than 30 wt %.[32] Furthermore, we found that PdCu/S-1 has an acetylene conversion higher than that of PdCu@S-1 owing to their distinguishable catalyst structures. For the PdCu/S-1 catalyst, the Pd nanoparticles are mostly exposed on the zeolite external surface, which were easily accessible to the reactant molecules. However, the partial surface of Pd nanoparticles was blocked by the zeolite framework in PdCu@S-1. In addition, the PdCu alloyed nanoparticles would reduce the acetylene conversion but improve the ethylene selectivity.[17] The PdCu alloyed structure was easy to be formed in PdCu@S-1 but relatively difficult on the PdCu/S-1 catalyst due to Pd−Cu phase separation. These

features result in PdCu/S-1 being more active than PdCu@S-1. In addition, the $C_2H_4$ selectivity of PdCu/S-1 is higher than 90% with $C_2H_2$ conversion below 70%, but the selectivity was rapidly decreased with increasing $C_2H_2$ conversion (Figure 2 and Supporting Information Figure S10 and Table S1), which follows the scaling relationship.[19,33] This feature should be assigned to the strong adsorption of $C_2H_4$ on the Pd surface that accelerates the overhydrogenation to form $C_2H_6$, which is consistent with those of previous reports.[33−35]

The comparison was further performed using the mixed feed gas with the industrial composition (1 vol % $C_2H_2$/10 vol % $H_2$/30 vol % $C_2H_4$/59 vol % Ar, GHSV at 40000 mL $g^{-1}$ $h^{-1}$). In this case, abundant $C_2H_4$ exists that challenges the selective hydrogenation of $C_2H_2$. The competition between ethylene and acetylene adsorption on the metal surface strongly determines the catalytic selectivity.[18] Based on this feature, it is reasonable to conclude that the ethylene-rich atmosphere would benefit the ethylene adsorption that affects the acetylene adsorption to some extent, thus exhibiting reduced ethylene selectivity in the semihydrogenations. The catalytic data are summarized in Supporting Information Figures S11 and S12. The PdCu/S-1 always exhibited a $C_2H_4$ selectivity lower than 50% under the given reaction conditions, and it continuously decreased with an increase of the $C_2H_2$ conversion. For example, $C_2H_4$ selectivity of 16.4% was obtained with a full conversion of $C_2H_2$. In contrast, PdCu@S-1 exhibited significantly improved $C_2H_4$ selectivity under the equivalent test conditions, obtaining ∼80% selectivity to $C_2H_4$ under full conversion of $C_2H_2$, which is about 5-fold higher than that on PdCu/S-1 (Supporting Information Figures S11 and S12 and Table S2). These results decidedly evidence the improved catalytic performance of PdCu@S-1 in the semihydrogenation of $C_2H_2$, which should be strongly correlated with the zeolite fixed alloy structure.

To further demonstrate the importance of the zeolite fixed structure of PdCu@S-1 in improving the catalyst performance, we treated the as-synthesized PdCu@S-1 catalyst with hydrofluoric acid, which can partially destroy the S-1 crystals and make the PdCu species surroundings similar to those of PdCu/S-1. The XRD pattern of PdCu@S-1-HF exhibited peaks assigned to the typical MFI zeolite structure, and the well-maintained zeolite morphology was confirmed by SEM characterization (Supporting Information Figure S13a,b). TEM images of PdCu@S-1-HF showed abundant mesopores, which should be due to the partial removal of silica species in the zeolite framework (Supporting Information Figure S13c,d). These data demonstrate that the zeolite crystals were partially etched, but the MFI zeolite morphology was basically maintained. As shown in Supporting Information Figure S14, the HF-treated PdCu@S-1 showed a $C_2H_2$ conversion higher than that of PdCu@S-1 under the equivalent reaction conditions, but the selectivity for $C_2H_4$ was reduced, indicating the importance of the zeolite sheath for selectively obtaining $C_2H_4$.

The durability of PdCu@S-1 and PdCu/S-1 was evaluated in the continuous semihydrogenation reactions (Supporting Information Figure S15). The conversion decreased slightly, but selectivity was maintained at about 95% for 10 h at 150 °C. Notably, the PdCu alloyed structure and the NPs mean size (3.8 nm) are basically unchanged for the used PdCu@S-1 (Supporting Information Figure S16). In the PdCu@S-1-catalyzed acetylene hydrogenation, the deactivation should be assigned to the coke formation that blocks the zeolite micropores, as confirmed by the TG analysis (Supporting Information Figure S17). In contrast, the acetylene conversion over PdCu/S-1 dropped to about half of the initial value under the same conditions (Supporting Information Figure S15b) because of the rapid Pd nanoparticle sintering, as confirmed by the TEM characterization (Supporting Information Figure S18). Nevertheless, the rigid zeolite framework would immobilize the metal nanoparticles to suppress the migration and ripening, thus stabilizing the metal nanoparticles under harsh reaction conditions. These data verify the excellent durability of the PdCu@S-1 catalyst in $C_2H_2$ semihydrogenation, which remarkably outperforms the traditional supported alloy catalysts that are easy to agglomerate or decompose under reaction conditions.

## Mechanism Study

To gain insights into the vast selectivity difference between PdCu@S-1 and other catalysts, XPS characterization was employed to study the electronic structure of these catalysts. As shown in Supporting Information Figure S19, the Pd 3d XPS signals are almost undetectable for PdCu@S-1, Pd@S-1, and PdCu/S-1 samples, which should be due to the low loading amount and/or fixation of Pd in zeolite crystals, which is very consistent with previous results because XPS is a surface technique.[36,37]

Figure 3a illustrates Cu 2p XPS spectra of PdCu@S-1, Cu@S-1, and PdCu/S-1 samples, and a relatively higher Cu loading (~0.8 wt %, Table 1) enables the detection of the charge state of Cu (the subsurface Cu species within the detection depth of XPS) and study on the electron transfer between Cu and Pd. Cu@S-1 exhibits a Cu $2p_{3/2}$ binding energy at 933.5 eV assigned to the $Cu^+/Cu^0$ species.[38,39] For PdCu@S-1, the Cu $2p_{3/2}$ peak is blue-shifted to 934.4 eV, suggesting a more positively charged Cu.[40] The PdCu/S-1 showed a Cu $2p_{3/2}$
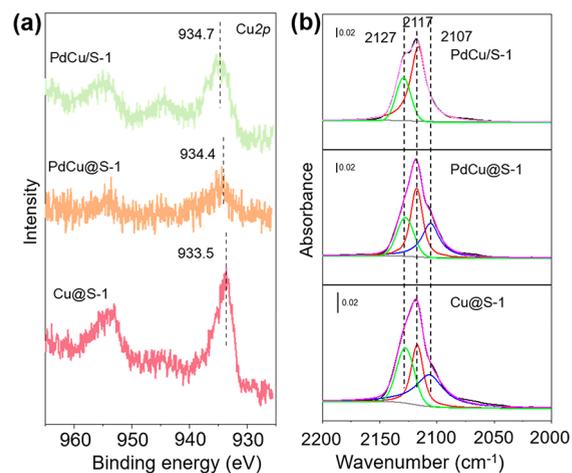


**Figure 3.** (a) Cu 2p XP spectra and (b) in situ CO adsorption FTIR spectra for Cu@S-1, PdCu@S-1, and PdCu/S-1 catalysts.

peak at 934.7 and a satellite peak at 944.7 eV, indicating that $Cu^{2+}$ is dominant. Notably, a more positively charged Cu species in PdCu@S-1 than in Cu@S-1 indicates the charge transfer between Cu and Pd via the alloy structure (Figure 1c), which can lead to an electron-enriched surface of Pd in PdCu@S-1.[17,29,36]

The electronic structures of the catalysts and Pd–Cu interactions were further investigated by in situ FTIR spectroscopy using CO as a probing molecule. As shown in Figure 3b, PdCu@S-1 showed a dominant peak at 2117 cm$^{-1}$ and two weak shoulders at 2127 and 2107 cm$^{-1}$ (Supporting Information Figure S20 and Table S3), which are assigned to $Cu^+$, partially reduced CuO, and metallic Cu species, respectively.[37,41] The signals of adsorbed CO was almost undetectable on Pd@S-1 due to the low loading of Pd and the fixed structures with partially blocked metal surface by the zeolite framework (Supporting Information Figure S21). The Cu@S-1 exhibited stronger CO adsorption on the $Cu^0$ species compared to that of PdCu@S-1 (Figure 3b and Supporting Information Figure S22 and Table S3). In contrast, PdCu/S-1 showed an enhanced intensity of signal at 2127 cm$^{-1}$ (Figure 3b and Supporting Information Figure S23 and Table S3), confirming a more positively charged Cu in PdCu/S-1, in good agreement with the XPS results. In brief, both XPS and CO-adsorbed FTIR spectra reveal that the Pd species are more negatively charged in PdCu@S-1 than those in Pd@S-1, leading to the electron-enriched Pd surface that could weaken the $C_2H_4$ adsorption because of the enhanced Pd d-electron back-donation to $C_2H_4$.[42,43] It is reasonable to imagine that such a feature should benefit the rapid product escape once the $C_2H_4$ is formed on the Pd surface to hinder the over-hydrogenation.

To understand the interactions of $C_2H_2$ and different intermediates with the catalysts' surface, in situ FTIR spectra of $C_2H_2$ adsorption over PdCu@S-1 and PdCu/S-1 were recorded. In a standard run, the PdCu@S-1 catalyst was pretreated with gaseous hydrogen, and then $C_2H_2$ was introduced at 150 °C. As shown in Figure 4a,b, the weakly adsorbed $C_2H_2$ by a hydrogen bond (1941 cm$^{-1}$) was detected.[44,45] Meanwhile, *CH═CH$_2$ species (2922, 1721, and 1710 cm$^{-1}$) were formed through a primary hydrogenation of $C_2H_2$.[44,46] The bands of gaseous $C_2H_4$ (3016 and 2969 cm$^{-1}$) were detected, indicating the successful hydrogenation
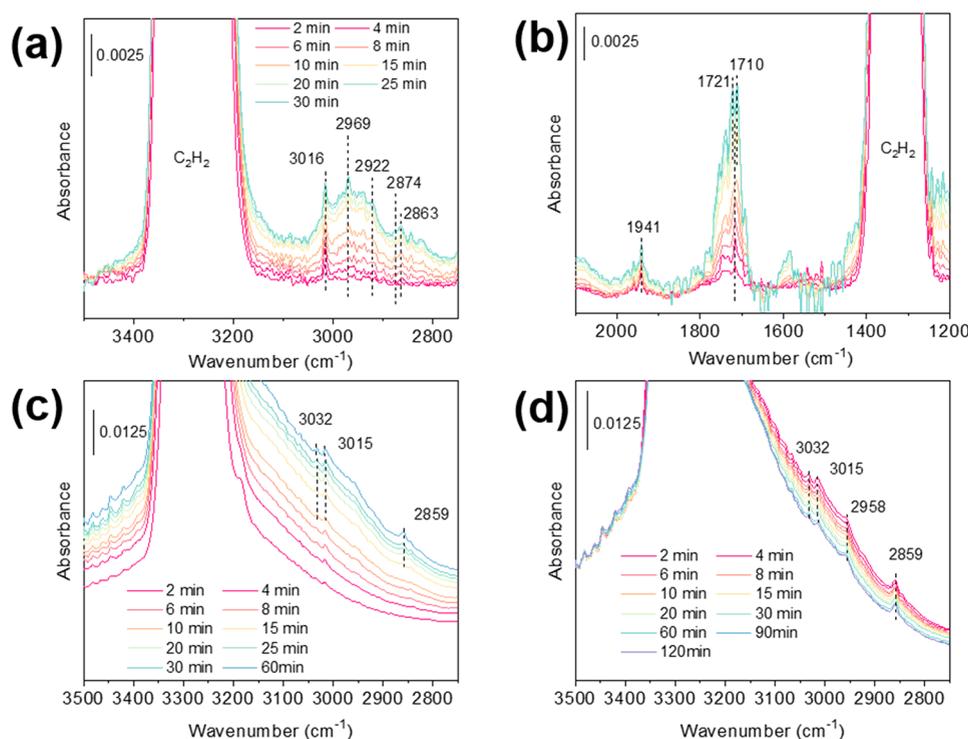
**Figure 4.** In situ FTIR spectra of $C_2H_2$ adsorption over (a,b) PdCu@S-1 and (c) PdCu/S-1 catalyst at 150 °C. (d) In situ FTIR spectra of $C_2H_2$ and hydrogen coadsorption over PdCu/S-1 at 150 °C.

of *CH=CH$_2$ species to $C_2H_4$.[47] The signals of $C_2H_6$ (2874 and 2863 cm$^{-1}$) were extremely weak, suggesting the high selectivity to $C_2H_4$ with hindered overhydrogenation, which are similar to those in catalytic results (Figure 2). Co-feeding of $C_2H_2$ and $H_2$ into PdCu@S-1 led to obvious signals of $C_2H_4$ (3016 and 2969 cm$^{-1}$), while characteristic peaks of $C_2H_6$ (2874 and 2863 cm$^{-1}$) were not observed (Supporting Information Figure S24), proving the high $C_2H_4$ selectivity of PdCu@S-1. For PdCu/S-1(Figure 4c,d), with the introduction of $C_2H_2$ and $H_2$, the characteristic peak of $C_2H_4$ (3015 cm$^{-1}$) appears first, then $C_2H_6$ (3032, 2958, and 2859 cm$^{-1}$) gradually formed, indicating the deep hydrogenation of $C_2H_4$ to $C_2H_6$. These results significantly reveal the superior $C_2H_4$ selectivity of PdCu@S-1, where both the PdCu alloy species and the zeolite fixed structure are important (Figure 5). We further explored the sorption of $C_2H_2$ and $C_2H_4$ on PdCu@S-1, which has been regarded as a crucial factor to determine the catalytic selectivity in semihydrogenation. As shown in the temperature-programmed desorption (TPD) profiles of the PdCu@S-1 catalyst (Supporting

Information Figure S25), the desorption signals of $C_2H_2$ were clearly observable, whereas the signal of $C_2H_4$ was almost undetectable. This feature would benefit the rapid $C_2H_4$ desorption to avoid the overhydrogenation.

## CONCLUSIONS

In summary, we reported the siliceous zeolite fixed PdCu alloy NPs as highly active and selective catalysts for semi-hydrogenation of $C_2H_2$, simultaneously giving high activity, selectivity, and durability to outperform the generally supported PdCu catalyst and Cu-free Pd@S-1 catalyst. The mechanism investigation reveals that the stabilized PdCu alloy structure benefits the rapid escape of $C_2H_4$ product to minimize the overhydrogenation. In addition, compared with the previous zeolite-based catalysts for semihydrogenation, dominantly the metal-exchanged aluminosilicate zeolite, this work demonstrates a new catalyst series with siliceous zeolites to avoid the possible acid-catalyzed oligomerization on aluminosilicate zeolite. This strategy reported here might offer a new route for designing new catalysts for semi-hydrogenations.

## ASSOCIATED CONTENT

### Supporting Information

The Supporting Information is available free of charge at https://pubs.acs.org/doi/10.1021/acsmaterialsau.1c00080.

Details for XRD, ICP, XPS, TG, TPD, and TEM characterizations, catalyst structure characterizations (XRD, N$_2$ sorption isotherms, SEM, and TEM), electronic structure characterizations (XPS and in situ FTIR), and catalytic performances ($C_2H_2$ conversion, $C_2H_4$ selectivity, and stability) (PDF)
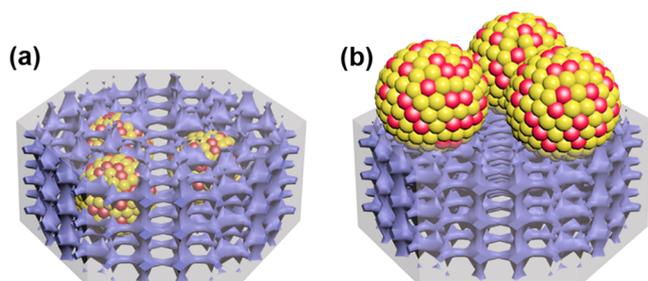


**Figure 5.** Simplified models of (a) PdCu@S-1 and (b) PdCu/S-1 (Pd, red; Cu, yellow).

## AUTHOR INFORMATION

### Corresponding Authors

**Feng-Shou Xiao** − *Key Lab of Biomass Chemical Engineering of Ministry of Education, College of Chemical and Biological Engineering, Zhejiang University, Hangzhou 310027, China*; Email: fsxiao@zju.edu.cn

**Liang Wang** − *Key Lab of Biomass Chemical Engineering of Ministry of Education, College of Chemical and Biological Engineering, Zhejiang University, Hangzhou 310027, China*; orcid.org/0000-0002-5826-1866; Email: liangwang@zju.edu.cn

### Authors

**Qingsong Luo** − *Key Lab of Biomass Chemical Engineering of Ministry of Education, College of Chemical and Biological Engineering, Zhejiang University, Hangzhou 310027, China*

**Hai Wang** − *Key Lab of Biomass Chemical Engineering of Ministry of Education, College of Chemical and Biological Engineering, Zhejiang University, Hangzhou 310027, China*

Complete contact information is available at:
https://pubs.acs.org/10.1021/acsmaterialsau.1c00080

### Author Contributions

[†]Q.L. and H.W. contributed equally to this work.

### Notes

The authors declare no competing financial interest.

## ACKNOWLEDGMENTS

## REFERENCES

(1) Ngamsom, B.; Bogdanchikova, N.; Avalos Borja, M.; Praserthdam, P. Characterisations of Pd−Ag/Al$_2$O$_3$ catalysts for selective acetylene hydrogenation: effect of pretreatment with NO and N$_2$O. *Catal. Commun.* 2004, 5, 243−248.

(2) Chan, C.; Mahadi, A. H.; Li, M. J.; Corbos, E. C.; Tang, C.; Jones, G.; Kuo, W. C. H.; Cookson, J.; Brown, C. M.; Bishop, P. T.; Tsang, S. C. E. Erratum: Interstitial modification of palladium nanoparticles with boron atoms as a green catalyst for selective hydrogenation. *Nat. Commun.* 2014, 5, 5787−5795.

(3) Teschner, D.; Révay, Z.; Borsodi, J.; Hävecker, M.; Knop-Gericke, A.; Schlögl, R.; Jackson, S. D.; Torres, D.; Sautet, P.; Milroy, D. Understanding palladium hydrogenation catalysts: when the nature of the reactive molecule controls the nature of the catalyst active phase. *Angew. Chem., Int. Ed.* 2008, 47, 9274−9278.

(4) Kim, W. J.; Kang, J. H.; Ahn, I. Y.; Moon, S. H. Effect of potassium addition on the properties of a TiO$_2$-modified Pd catalyst for the selective hydrogenation of acetylene. *Appl. Catal. A: Gen.* 2004, 268, 77−82.

(5) Sheth, P. A.; Neurock, M.; Smith, C. M. First-Principles analysis of the effects of alloying Pd with Ag for the catalytic hydrogenation of acetylene-mixtures. *J. Phys. Chem. B* 2005, 109, 12449−12466.

(6) Cao, X.; Mirjalili, A.; Wheeler, J.; Xie, W.; Jang, B. W.-L. Investigation of the preparation methodologies of Pd-Cu single atom alloy catalysts for selective hydrogenation of acetylene. *Front. Chem. Sci. Eng.* 2015, 9, 442−449.

(7) Guo, Z.; Liu, Y. Y.; Liu, Y. Y.; Chu, W. Promising SiC support for Pd catalyst in selective hydrogenation of acetylene to ethylene. *Appl. Surf. Sci.* 2018, 442, 736−741.

(8) Zhang, L.; Zhou, M.; Wang, A.; Zhang, T. Selective Hydrogenation over Supported Metal Catalysts: From Nanoparticles to Single Atoms. *Chem. Rev.* 2020, 120, 683−733.

(9) Zhang, Z.; Peh, S. B.; Wang, Y.; Kang, C.; Fan, W.; Zhao, D. Efficient Trapping of Trace Acetylene from Ethylene in an Ultramicroporous Metal−Organic Framework: Synergistic Effect of High-Density Open Metal and Electronegative Sites. *Angew. Chem., Int. Ed.* 2020, 59, 18927−18932.

(10) Liu, Y. X.; Liu, X. W.; Feng, Q. C.; He, D. S.; Zhang, L. B.; Lian, C.; Shen, R. G.; Zhao, G. F.; Ji, Y. J.; Wang, D. S.; Zhou, G.; Li, Y. D. *Adv. Mater.* 2016, 28, 4747−4754.

(11) McCue, A. J.; Anderson, J. A. Recent advances in selective acetylene hydrogenation using palladium containing catalysts. *Front Chem. Sci. Eng.* 2015, 9, 142−153.

(12) García-Mota, M.; Bridier, B.; Pérez-Ramírez, J.; López, N. J. Interplay between carbon monoxide, hydrides, and carbides in selective alkyne hydrogenation on palladium. *J. Catal.* 2010, 273, 92−102.

(13) Crespo-Quesada, M.; Yarulin, A.; Jin, M.; Xia, Y.; Kiwi-Minsker, L. Structure sensitivity of alkynol hydrogenation on shape- and size-controlled palladium nanocrystals: which sites are most active and selective? *J. Am. Chem. Soc.* 2011, 133, 12787−12794.

(14) Pei, G. X.; Liu, X. Y.; Wang, A. Q.; Lee, A. F.; Isaacs, M. A.; Li, L.; Pan, X. L.; Yang, X. F.; Wang, X. D.; Tai, Z. J.; Wilson, K.; Zhang, T. Ag alloyed Pd single-atom catalysts for efficient selective hydrogenation of acetylene to ethylene in excess ethylene. *ACS Catal.* 2015, 5, 3717−3725.

(15) Lee, J. H.; Kim, S. K.; Ahn, I. Y.; Kim, W.-J.; Moon, S. H. Performance of Pd−Ag/Al$_2$O$_3$ catalysts prepared by the selective deposition of Ag onto Pd in acetylene hydrogenation. *Catal. Commun.* 2011, 12, 1251−1254.

(16) Han, Y.; Peng, D.; Xu, Z.; Wan, H.; Zheng, S.; Zhu, D. TiO$_2$ supported Pd@Ag as highly selective catalysts for hydrogenation of acetylene in excess ethylene. *Chem. Commun.* 2013, 49, 8350−8352.

(17) Pei, G. X.; Liu, X. Y.; Yang, X.; Zhang, L.; Wang, A.; Li, L.; Wang, H.; Wang, X.; Zhang, T. Performance of Cu-alloyed Pd single-atom catalyst for semihydrogenation of acetylene under simulated front-end conditions. *ACS Catal.* 2017, 7, 1491−1500.

(18) Zhou, H.; Yang, X.; Li, L.; Liu, X.; Huang, Y.; Pan, X.; Wang, A.; Li, J.; Zhang, T. PdZn intermetallic nanostructure with Pd−Zn−Pd ensembles for highly active and chemoselective semi-hydrogenation of acetylene. *ACS Catal.* 2016, 6, 1054−1061.

(19) Ding, L. B.; Yi, H.; Zhang, W. H.; You, R.; Cao, T.; Yang, J. L.; Lu, J. L.; Huang, W. X. Activating edge sites on Pd catalysts for selective hydrogenation of acetylene via selective Ga$_2$O$_3$ decoration. *ACS Catal.* 2016, 6, 3700−3707.

(20) Armbrüster, M.; Wowsnick, G.; Friedrich, M.; Heggen, M.; Cardoso-Gil, R. Synthesis and catalytic properties of nanoparticulate intermetallic Ga−Pd compounds. *J. Am. Chem. Soc.* 2011, 133, 9112−9118.

(21) Cao, Y.; Sui, Z.; Zhu, Y.; Zhou, X.; Chen, D. Selective hydrogenation of acetylene over Pd-In/Al$_2$O$_3$ catalyst: promotional effect of indium and composition-dependent performance. *ACS Catal.* 2017, 7, 7835−7846.

(22) Feng, Q.; Zhao, S.; Wang, Y.; Dong, J.; Chen, W.; He, D.; Wang, D.; Yang, J.; Zhu, Y.; Zhu, H.; Gu, L.; Li, Z.; Liu, Y.; Yu, R.; Li, J.; Li, Y. Isolated single-atom Pd sites in intermetallic nanostructures: high catalytic selectivity for semihydrogenation of alkynes. *J. Am. Chem. Soc.* 2017, 139, 7294−7301.

(23) Ma, C.; Du, Y. Y.; Feng, J. T.; Cao, X. Z.; Yang, J.; Li, D. Q. Fabrication of supported PdAu nanoflower catalyst for partial hydrogenation of acetylene. *J. Catal.* 2014, 317, 263−271.

(24) Wang, Y. F.; Hall, A. S. Pulsed electrodeposition of metastable Pd$_{31}$Bi$_{12}$ nanoparticles for oxygen reduction electrocatalysis. *ACS Energy Lett.* 2020, 5, 17−22.

(25) Sun, D.; Wang, Y. f.; Livi, K. J. T.; Wang, C. H.; Luo, R. C.; Zhang, Z. Q.; Alghamdi, H.; Li, C. Y.; An, F. F.; Gaskey, B.; Mueller, T.; Hall, A. S. Ordered intermetallic Pd$_3$Bi prepared by an

electrochemically induced phase transformation for oxygen reduction electrocatalysis. *ACS Nano* **2019**, *13*, 10818−10825.

(26) Osswald, J.; Giedigkeit, R.; Jentoft, R. E.; Armbrüster, M.; Girgsdies, F.; Kovnir, K.; Ressler, T.; Grin, Y.; Schlögl, R. Palladium−gallium intermetallic compounds for the selective hydrogenation of acetylene: part I: preparation and structural investigation under reaction conditions. *J. Catal.* **2008**, *258*, 210−218.

(27) Yang, J.; Zhang, F. J.; Lu, H. Y.; Hong, X.; Jiang, H. L.; Wu, Y.; Li, Y. D. Hollow Zn/Co ZIF particles derived from core−shell ZIF-67@ZIF-8 as selective catalyst for the semi-hydrogenation of acetylene. *Angew. Chem., Int. Ed.* **2015**, *127*, 11039−11043.

(28) Liu, L. C.; Lopez-Haro, M.; Lopes, C. W.; Li, C. G.; Concepcion, P.; Simonelli, L.; Calvino, J. J.; Corma, A. Regioselective generation and reactivity control of subnanometric platinum clusters in zeolites for high-temperature catalysis. *Nat. Mater.* **2019**, *18*, 866−873.

(29) Sun, Q. M.; Chen, B. W. J.; Wang, N.; He, Q.; Chang, A.; Yang, C.-M.; Asakura, H.; Tanaka, T.; Hülsey, M. J.; Wang, C.-H.; Yu, J. H.; Yan, N. Zeolite-Encaged Pd−Mn Nanocatalysts for $CO_2$ Hydrogenation and Formic Acid Dehydrogenation. *Angew. Chem., Int. Ed.* **2020**, *132*, 20358−20366.

(30) Liu, L. C.; Lopez-Haro, M.; Lopes, C. W.; Meira, D. M.; Concepcion, P.; Calvino, J. J.; Corma, A. Atomic-level understanding on the evolution behavior of subnanometric Pt and Sn species during high-temperature treatments for generation of dense PtSn clusters in zeolites. *J. Catal.* **2020**, *391*, 11−24.

(31) Pei, G. X.; Liu, X. Y.; Yang, X. F.; Zhang, L. L.; Wang, A. Q.; Li, L.; Wang, H.; Wang, X. D.; Zhang, T. Performance of Cu-alloyed Pd single-atom catalyst for semihydrogenation of acetylene under simulated front-end conditions. *ACS Catal.* **2017**, *7*, 1491−1500.

(32) Bridier, B.; Perez-Ramirez, J. Cooperative effects in ternary Cu-Ni-Fe catalysts lead to enhanced alkene selectivity in alkyne hydrogenation. *J. Am. Chem. Soc.* **2010**, *132*, 4321−4327.

(33) Zou, S.; Lou, B.; Yang, K.; Yuan, W.; Zhu, C.; Zhu, Y.; Du, Y.; Lu, L.; Liu, J.; Huang, W.; Yang, B.; Gong, Z.; Cui, Y.; Wang, Y.; Ma, L.; Ma, J.; Jiang, Z.; Xiao, L.; Fan, J. Grafting nanometer metal/oxide interface towards enhanced low-temperature acetylene semi-hydrogenation. *Nat. Commun.* **2021**, *12*, 5770.

(34) Crespo-Quesada, M.; Yarulin, A.; Jin, M. S.; Xia, Y. N.; Kiwi-Minsker, L. Structure sensitivity of alkynol hydrogenation on shape- and size-controlled palladium nanocrystals: which sites are most active and selective? *J. Am. Chem. Soc.* **2011**, *133*, 12787−12794.

(35) Hamm, G.; Schmidt, T.; Breitbach, J.; Franke, D.; Becker, C.; Wandelt, K. The Adsorption of Ethene on Pd (111) and Ordered Sn/Pd (111) Surface Alloys. *Z. Phys. Chem.* **2009**, *223*, 209−232.

(36) Ball, M. R.; Rivera-Dones, K. R.; Gilcher, E. B.; Ausman, S. F.; Hullfish, C. W.; Lebrón, E. A.; Dumesic, J. A. AgPd and CuPd catalysts for selective hydrogenation of acetylene. *ACS Catal.* **2020**, *10*, 8567−8581.

(37) Kang, L.; Wang, B.; Guntner, A. T.; Xu, S.; Wan, X.; Liu, Y.; Marlow, S.; Ren, Y.; Gianolio, D.; Tang, C. C.; Murzin, V.; Asakura, H.; He, Q.; Guan, S.; Velasco-Velez, J. J.; Pratsinis, S. E.; Guo, Y.; Wang, F. R. The Electrophilicity of Surface Carbon Species in the Redox Reactions of $CuO$-$CeO_2$ Catalysts. *Angew. Chem., Int. Ed.* **2021**, *60*, 14420−14428.

(38) Tseng, I. H.; Wu, J. C. S.; Chou, H. Y. Effects of Sol-gel Procedures on the Photocatalysis of $Cu/TiO_2$ in $CO_2$ Photoreduction. *J. Catal.* **2004**, *221*, 432−440.

(39) Espinos, J. P.; Morales, J.; Barranco, A.; Caballero, A.; Holgado, J.; Gonzalez-Elipe, A. Interface Effects for Cu, CuO, and $Cu_2O$ Deposited on $SiO_2$ and $ZrO_2$. XPS Determination of the Valence State of Copper in $Cu/SiO_2$ and $Cu/ZrO_2$ Catalysts. *J. Phys. Chem. B* **2002**, *106*, 6921−6929.

(40) Shi, X. X.; Lin, Y.; Huang, L.; Sun, Z. H.; Yang, Y.; Zhou, X. H.; Vovk, E.; Liu, X. Y.; Huang, X. H.; Sun, M.; Wei, S. Q.; Lu, J. L. Copper catalysts in semihydrogenation of acetylene: from single atoms to nanoparticles. *ACS Catal.* **2020**, *10*, 3495−3504.

(41) Yu, J.; Sun, X.; Tong, X.; Zhang, J.; Li, J.; Li, S.; Liu, Y.; Tsubaki, N.; Abe, T.; Sun, J. Ultra-high thermal stability of sputtering reconstructed Cu-based catalysts. *Nat. Commun.* **2021**, *12*, 7209.

(42) Ding, K. L.; Gulec, A.; Johnson, A. M.; Schweitzer, N. M.; Stucky, G. D.; Marks, L. D.; Stair, P. C. Identification of active sites in CO oxidation and water-gas shift over supported Pt catalysts. *Science* **2015**, *350*, 189−192.

(43) Liu, S. F.; Qi, H. F.; Zhou, J. H.; Xu, W.; Niu, Y. M.; Zhang, B. S.; Zhao, Y.; Liu, W.; Ao, Z. M.; Kuang, Z. C.; Li, L.; Wang, M.; Wang, J. H. Encapsulation of Platinum by Titania under an Oxidative Atmosphere: Contrary to Classical Strong Metal−Support Interactions. *ACS Catal.* **2021**, *11*, 6081−6090.

(44) Moon, J.; Cheng, Y. Q.; Daemen, L. L.; Li, M. J.; Polo-Garzon, F.; Ramirez-Cuesta, A. J.; Wu, Z. L. Discriminating the role of surface hydride and hydroxyl for acetylene semihydrogenation over ceria through *in situ* neutron and infrared spectroscopy. *ACS Catal.* **2020**, *10*, 5278−5287.

(45) Ivanov, A. V.; Koklin, A. E.; Uvarova, E. B.; Kustov, L. M. A DRIFT spectroscopic study of acetylene adsorbed on metal oxides. *Phys. Chem. Chem. Phys.* **2003**, *5*, 4718−4723.

(46) Cao, T.; You, R.; Zhang, X.; Chen, S.; Li, D.; Zhang, Z.; Huang, W. An *in situ* DRIFTS mechanistic study of $CeO_2$-catalyzed acetylene semihydrogenation reaction. *Phys. Chem. Chem. Phys.* **2018**, *20*, 9659−9670.

(47) Chai, Y. C.; Wu, G. J.; Liu, X. Y.; Ren, Y. J.; Dai, W. L.; Wang, C. M.; Xie, Z. K.; Guan, N. J.; Li, L. D. Acetylene-selective hydrogenation catalyzed by cationic nickel confined in zeolite. *J. Am. Chem. Soc.* **2019**, *141*, 9920−9927.